J MATER RES TECHNOL. 2020;9(6):13729–13739

Available online at www.sciencedirect.com

jmr&t Journal of Materials Research and Technology

https://www.journals.elsevier.com/journal-of-materials-research-and-technology

Original Article

Ecofriendly production of bioactive tissue engineering scaffolds derived from egg- and sea-shells

Vincent Hembrick-Holloman[a,1,2], *Temesgen Samuel*[b,1,2], *Zaheeruddin Mohammed*[a,1,2], *Shaik Jeelani*[a,1,2], *Vijaya K. Rangari*[a,*,1,2]

[a] *Department of Material Science and Engineering, Tuskegee University, Tuskegee, AL 36088, United States*
[b] *Department of Pathobiology, College of Veterinary Medicine, Nursing and Allied Health, Tuskegee University, Tuskegee, AL 36088, United States*

ARTICLE INFO

Article history:
Received 6 July 2020
Accepted 24 September 2020
Available online 3 October 2020

Keywords:
3D printing
Bioprinting
Hydroxyapatite
Bioinks
Bioactivity
Tissue engineering
3D printed scaffolds

ABSTRACT

Managing the vast amounts of eggshell and sea-shell waste that is produced globally each year is becoming very problematic as this material is simply disposed of in landfills. This waste results in odor production and microbial growth directly leading to environmental stresses. Transforming this waste into valuable biomaterials pose significant environmental and economic advantages as discarded waste have materials that can be utilized. The objective of this work was to develop inexpensive, bioactive hydroxyapatite-based scaffolds for tissue engineering applications by using an eco-friendly and sustainable approach. Engineering nano hydroxyapatite (EnHA) was derived from chicken eggshell and clam sea-shell waste by using an energy efficient microwave assisted wet chemical precipitation method. X-ray diffraction (XRD), Field emission scanning electron microscopy (FESEM), Transmission electron microscopy (TEM), and Energy dispersive spectroscopy (EDS) were used to analyze the biomaterials. Results show that the particles are highly crystalline hydroxyapatite (HA) with acicular shapes and within nanometer size ranges. The chemical compositions match exactly that of naturally occurring HA. The EnHA infused polymer scaffolds were fabricated using slurry-based solution 3D printing techniques. The slurry solutions composed of 70 wt% EnHA and 30 wt% Polycarpolactone (PCL). The XRD, SEM, EDS, and in vitro cell studies were conducted to determine the ability of the scaffolds to support cell adhesion and maintain viability. The scaffolds supported cellular attachment and maintenance when observed over a period of several days, suggesting their potential for future tissue regeneration research and applications.

* *Corresponding author.*
E-mail: vrangari@tuskegee.edu (V.K. Rangari).
[1] The authors contributed equally to this paper and shared first authorship.
[2] The authors contributed equally to this paper and shared last authorship.
https://doi.org/10.1016/j.jmrt.2020.09.093

1. Introduction

The ability to manage the enormous amounts of waste produced by the food processing industry is a challenging problem [1]. To produce a sustainable economy and environment, scientists and engineers must develop processes that focus on reducing, reusing, and recycling. By utilizing the naturally occurring minerals within waste, this hazardous waste can be converted into valuable nano-biomaterials. This results in an eco-friendly, environmentally sustainable process that can produce nano-biomaterials for tissue engineering applications [2,3]. The relationship between biomaterials and renewable resources has emerged as a promising opportunity in the development of novel manufacturing strategies within the past few years.

Eggshells and seashells are key examples of product-specific waste in the food processing industry that still harbor utilizable parts when discarded as waste [4]. As this waste is considered useless, most is disposed of in landfills without any thought of utilizing the waste as a valuable material. The management of this waste poses direct environmental and economic stresses as it leads to increased disposal costs, the risk of propagation of pathogens, along with unpleasant odors. Discarded eggshell is an environmental nuisance that generates 8 million tons of waste per year around the world [5]. China alone has to dispose of 10 million tons of shellfish waste annually. This waste mostly consists of oyster, clam, scallop, and mussel shells which are mostly disposed of in landfills. To reduce the environmental and economic stresses, these waste materials can be converted into EnHA that can be used as valuable bioactive fillers within tissue engineering scaffolds [6,7].

Engineered nanomaterials are of interest for biomedical applications due to their unique physical, chemical, biological and mechanical properties [8,9]. The interaction between manufactured nanoparticles and the biological environment are not fully understood and must be studied further. Not understanding the effects of nanoparticles on cell viability is a significant barrier when it comes time to apply these nanoparticles in medicine and biology. Factors such as starting material, manufacturing process, particle size, shape, crystallinity or chemical composition all have different impacts on the adverse of effects of nanomaterials on living organisms [10–12]. Our study wanted to investigate how the EnHA extracted from each respective waste source differed when it came to the interactions between the extracted bioactive fillers and osteoblast cells.

Tissue engineering is a technology that uses harvested cells from a patient and seeds them onto customizable scaffolds to later be implanted into the patient [13]. Scaffolds are used as artificial templates to create a 3D environment that is intended to promote cellular attachment, migration, proliferation and differentiation. Synthetic polymers such as poly(glycolic acid) (PGA), poly(lactic acid) (PLA), poly(ethylene glycol) (PEG), and poly(caprolactone) (PCL) have been used to create scaffolds [14–17]. However, the biological and mechanical properties of these synthetic polymers are not satisfactory for tissue engineering applications when used alone. Fillers and reinforced materials that improve the mechanical properties are known to have inherently low levels of biocompatibility.

Egg- and seashells possess a natural mineral know as calcium carbonate which can be used to extracted and used to convert into a valuable bioactive material known as hydroxyapatite (HA). HA, with the chemical composition of $Ca_{10}(PO4)_6(OH)_2$, is a very promising biomaterial, as it serves as the prime inorganic constituent (65–70%) of bone and hard tissue matrix. HA is popular within the biomedical community because it has two active binding sites, Ca^{2+} and PO_4^{3-}. These sites have proven to be favorable and possess affinity toward biological macromolecules. Additionally, HA possesses valuable properties for tissue engineering, which include biocompatibility, osteoconductivity, nontoxicity, and bioactivity. Previous studies have shown that HA is a promising biomaterial that can be used as a replacement filler in scaffolds for tissue engineering applications. However, nanoscale HA is known to be expensive due to the use of high purity metals and reagents used to produce it [18–20]. Additionally, synthetic HA produced from chemicals such as CaO, $Ca(NO_3)_2$, $(NH_4)HPO_4$ donot possess adequate biological properties versus naturally occurring HA that is extracted from natural sources. By utilizing this waste to produce EnHA a solution is proposed that can reduce the production cost of HA while also improving the biological properties at the same time.

The objective of this research is to develop a unique and sustainable approach to fabricate complex 3D scaffolds for tissue engineering applications. Traditional methods such as salt-leaching, freeze-drying, gas forming, and phase separation have been used to fabricate 3D scaffolds for tissue regeneration. However, these methods are limited by their inability to precisely control the internal scaffold architecture or construct highly complex structures. Because of these limitations, 3D printing gained interest and growth as an attractive alternative. 3D printing technology creates objects layer by layer to create a 3D volumetric structure. Producing scaffolds in this manner provides the ability to create highly complex, customizable structures that can fine-tune the properties of biomaterial-based scaffolds [21–23]. Although, 3D fabrication method shows much promise, there are still limitations that remain. To date, there are only a limited number of biomaterials that can be 3D processed and fabricated in comparison to the traditional techniques mentioned above [24]. To our knowledge, our work is the first customizable extrusion-based 3D printing technique to fabricate complex hydroxyapatite-based scaffolds with a weight percentage of up to 70%. In the current study, we developed composite scaffolds from nanocrystalline hydroxyapatite and polycaprolactone by using an inexpensive and environmentally friendly 3D printing method, with potential for orofacial and dental tissue regeneration applications.

2. Materials and methods

2.1. *Materials*

Raw white Eggshells were provided by American Dehydrated Foods, Atlanta, GA. Raw and raw clam shells were procured from Atlanta international market, Atlanta, GA. Analytical

grade sodium hydroxide (NaOH) pellets, ethanol (99.5% purity, absolute), nitric acid (65% HNO_3), ammonium hydroxide (28% NH_4OH), semiconductor grade phosphoric acid (85% H_3PO_4), Dichloromethane (CH_2HCl_2) were purchased from Sigma-Aldrich Chemical, Allentown, PA. Milli-Q deionized (DI) water (resistivity, 18.2 MX.cm, Millipore RiOs and Elix water purification systems, Millipore Corporation, MA) was used throughout this research. Powdered Polycarpolactone (PCL) was purchased from Polysciences Inc, Washington, PA. All custom-built 3D printing (Hyrel 30M) and printing accessories used in this experiment was purchased from Hyrel 3D Printing Company located in Atlanta, GA.

2.2. Synthesis of nHA from raw shell waste

nHA was synthesized using a wet-precipitation method by utilizing $CaCO_3$ from egg and seashells and H_3PO_4 as the sources of calcium and phosphate ions. As-received shell waste was first boiled in deionized water overnight, followed by grinding in a commercial kitchen blender. The grinding was necessary to assist in helping to denature and decant the organic materials from the heavier inorganic materials. The inorganic sample was then pulverized again until a fine egg or seashell powder ($CaCO_3$) formed and passed through a 20-mm mesh sieve. Desired EnHA was synthesized by using $CaCO_3$ from each shell source as follows: 20 g of shell powder was added into an Erlenmeyer flask containing 28 mL of HNO_3 solution and magnetically stirred at 300 rpm for 30 min.

$$CaCO_3(s) + 2HNO_3(aq) \rightarrow Ca(NO_3)_2(s) + CO_2(g) + H_2O(l)$$

This resulted into a pale yellowish $Ca(NO_3)_2$ slurry. In the second step, diammonium hydrogen phosphate [$(NH_4)_2HPO_4$, DAHP] powder was synthesized by transferring 60 mL of NH_4OH into a stoichiometric amount of H_3PO_4 (15 mL) at a rate of 1 mL/min using a micropipette.

$$2NH_4OH(aq) + H_3PO_4(aq) \rightarrow (NH_4)2HPO_4(s) + 2H_2O(l)$$

Precipitated white DAHP powder was then filtered and washed thoroughly using a mixture of DI water and ethanol (1:1 v/v). In the third step, 3 g of $Ca(NO_3)_2$ was dissolved in 100 mL of DI water and stirred for 10 min at 400 rpm at a temperature of 40 °C while 2.4 g of DAHP was dissolved in 60 mL of DI water, separately. Aqueous DAHP solution was added drop-by-drop into the $Ca(NO_3)_2$ solution at the rate of 3 mL/min. NH_4OH was then added to the reaction mixture to adjust the pH to 11 after which it was stirred for 5 min.

$$10Ca(NO_3)_2(aq) + 6(NH_4)2HPO_4 + 8NH_4OH \rightarrow Ca_{10}(PO_4)_6OH_2 + 10NH_4NO_3$$

Finally, the reaction mixture was exposed to a microwave (45 microwave power) in an isothermal condition of 80 °C for 15 min. After cooling to RT, the white precipitated material was collected, washed using a mixture of ethanol and DI water, and centrifuged to remove any residual polymer and ammonium nitrate. The washing procedure was repeated three times and dried which is herein termed as "as-synthesized nHA". Three different forms of nHA were produced based on starting waste material: Eggshell (ESnHA), Littleneck Clam Shell (LNnHA) and Quahog Clam Shell (QSnHA).

2.3. Preparation of nHA based slurry for 3D printing

After the synthesis of nHA, particles were manually crushed in a mortar until a very fine powder was produced. The powder was then sieved through a 90-micrometer sieve to filter out larger particles and to ensure proper and consistent dispersion throughout the polymer matrix. The solution was prepared by dissolving 30 wt% of polycarpolactone in 30 mL of dichloromethane.

Next, 70 wt% nHA was slowly added and magnetically stirred into the solution for 3 h at 35 °C until an even distribution was achieved and it became a very thick solution with paste-like consistency. To ensure consistent mixing the addition of nHA did not begin until the polymer was completely dissolved within the solvent. 1 g of nHA was added every 3 min so that nHA particles did not clump up and agglomerate. A customizable extrusion-based 3D printing method was used to print slurry from each material. The solution was loaded into the extrudable syringe and then loaded onto the 3D printer (Fig. 1). nHA based scaffolds were printed at proportions of 70 wt% nHA and 30 wt% PCL.

2.4. Fabrication of 3D-printed hydroxyapatite based scaffold

The computer program, FreeCAD, was used to create 3D computer-aided models (CAD) of the printed scaffolds. The scaffolds created in FreeCAD were saved in a *.stl (stereolithography) file format, which describes the volume of surface mesh in a 3D space. The respective *.stl file was then uploaded into "Slic3r" program. This program is used to translate the 3D data by the printer, so that key parameters of the printing model could be customized and adjusted. These parameters include options such as nozzle diameter, layer height, printing speed, etc. Once the correct printing parameters in Slic3r were chosen, the file was converted into "G-Code", a code that directs the machine how to perform an action. A square scaffold measuring 2 cm length ×2 cm width ×2 cm height was printed with both 0°–90° and 0°–45° orientations to produce scaffolds with alternating layers.

A custom modified Hyrel 3D printer (Hyrel, Atlanta, Ga) with an EMO-25 extruder was used for fabrication. The G-code for nozzle movement was written to print a layered but highly porous structure that can allow the nutrient transport and cells to grow throughout the structure. The printing parameters such as filament spacing, layer height, and printing speed were identified based on visual inspection and optical microscopic images after the first and second layer printing for different paste compositions. The different printing results for the various weight concentrations of the solutions can be seen in Table 1. This printer head uses a stepping motor with gear reduction system designed to print materials such as clays, pastes, and adhesives at room temperature.

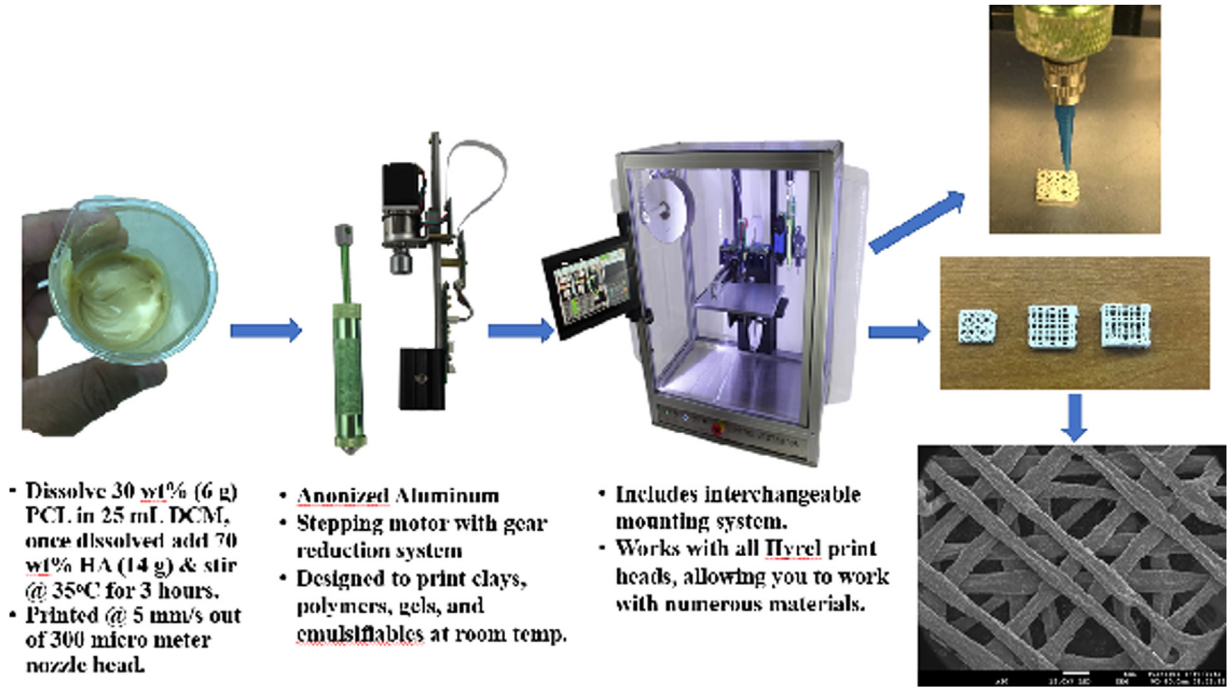

Fig. 1 – Flow Chart of 3D Printing Process. Hydroxyapatite (HA) based scaffolds were obtained by dissolving 30 wt% PCL in 25 mL dichloromethane. Once dissolved 70 wt% HA was added and magnetically stirred for 3 h at 35 °C. The slurry solution was then added to an anonized aluminum printing head and was printed at a rate of 5 mm/s out of a 300 micro meter nozzle head.

Table 1 – Printability of different solution compositions.

HA content (wt.%)	Bonded layers	Ease of handling	Printability	Comments
100	No	N/A	N/A	Solutions were too thick to be printed. Clogged printer nozzles.
70	Yes	Manageable	Printable and lead to the most uniform constructs.	Relatively easy printing but was not 100% precise.
60	Yes	Manageable	Printed uniform constructs.	Easy to print but wanted a higher HA wt%
50	Barely	Difficult	Viscous enough to be printed but could not print layers or complex structures.	Constructs could not print quick enough to produce complex 3D shapes.

2.5. *Characterization of synthesized nHA*

Phase analysis and the crystal structure of nHA was investigated using X-ray diffraction (XRD) using a Rigaku theta–theta powder diffractometer. The Cu-Ka radiation ($\lambda = 1.54$ Å) was used at a voltage of 40 kV and a current of 30 mA. The diffraction patterns were recorded in the range of 20–60° Bragg angles (2θ) at a scan rate of 2° min^{-1} with a step size of 0.02°. The XRD patterns and acquired peaks of synthesized nHA were analyzed using the Joint Committee on Powder Diffraction Standards (JCPDS) library.

Particle shape and morphology was observed using a JEOL JSM-7200F Field Emission Scanning Electron Microscope (SEM; FESEM, JEOL USA, Peabody, MA) at 10–20 kV. Samples were sputter coated with gold/palladium (Au/Pd) for 2–3 min before performing scanning electron microscopy (SEM).

Energy dispersive X-ray spectroscopy (EDS) was performed using a Bruker Energy dispersive spectrometer coupled with JEOL FESEM to find out the molar ratio of calcium/phosphorus of as-synthesized nHA.

Particle size and crystal structure of as-synthesized nHA was observed using a JEOL-2010 high-resolution transmission electron microscope (TEM; HRTEM, JEOL USA, Peabody, MA) at 150 kV. To prepare specimens for HRTEM imaging, as-synthesized nHA was ultrasonicated in ethanol for 5 min at RT and a drop was placed onto a carbon-coated copper grid and allowed to dry before HRTEM observation.

2.6. *Physiochemical characterization of nHA based 3D printed scaffolds*

The surface morphology and micro structural analysis was characterized by scanning electron microscopy and semi

quantitative elemental analysis was carried out using an EDS detector. SEM (JEOL JSM-7200F FESEM, JEOL USA, Peabody, MA) images were taken to evaluate the surface morphology of the scaffolds, internal structure of the filaments, and pore size with at least five measurements and the results were reported as mean ± standard deviation.

2.7. *Assessment of cell adhesion and growth on nHA-based scaffolds*

To examine the suitability of our 3D printed scaffolds to support cell adhesion and proliferation, human Osteoblast cells (hFOB, American Type Culture Collection (#CRL-11372), were used. Scaffolds that were tested for bioactivity were 30% PCL and 70% of each respective nHA. hFOB cells were cultured in growth media composed of Dulbecco's Modified Eagle Medium – High Glucose (DMEM) supplemented with fetal bovine serum (FBS) 1% (v/v) L-glutamine, and 10 μg/mL ciprofloxacin as antibacterial. Cells were incubated in a humidified incubator under routine cell culture conditions (37 °C, 5% CO_2/95% air environment). Each respective scaffold (ESnHA, LNnHA, QSnHA) was seeded with hFOB cells and studied over various time frames. All 3D printed scaffolds were sterilized in 70% ethanol for 30 min then washed three times in PBS before cell seeding. Seeded scaffolds were then incubated as above for various lengths of time (12 h, 24 h, 3 days or 5 days). Adhesion and spreading of cells were examined under a field emission scanning electron microscope. For SEM analysis, cell-seeded scaffold samples were fixed, dehydrated, vacuum-dried, and gold/palladium coated as described.

2.8. *Mechanical assessment of EnHA based scaffolds*

Mechanical tests were performed on 3D printed scaffolds with different reinforcements according to the ASTM D38822/D3822M-14 using Zwick Roell with a load cell capacity of 20 N. The tests were conducted at room temperature in displacement control at a constant crosshead speed of 0.5 mm/min. A minimum of five specimens were tested for each sample type. This test method was used to determine the elastic modulus, tensile strength and strain at failure of the material. The mechanical properties of scaffolds are important, as they need to support the tissue until it can support itself. Ideally scaffolds should be capable to combat the physiological stresses induced within them during implantation and should be in coherence with mechanical properties of target tissue.

3. Results & discussion

3.1. *Physiochemical characterization of synthesized nHA (ESnHA, LNnHA, QSnHA)*

A representative XRD pattern of as-synthesized ESnHA, LNnHA, and QSnHA are presented in Fig. 2(a–c). All obtained crystallographic information from the XRD diffractograms was compared with standards by the Joint Committee on Powder Diffraction and Standards (JCPDS). All the peaks matched closely with those of PDF standard card (00-009-0432) patterns

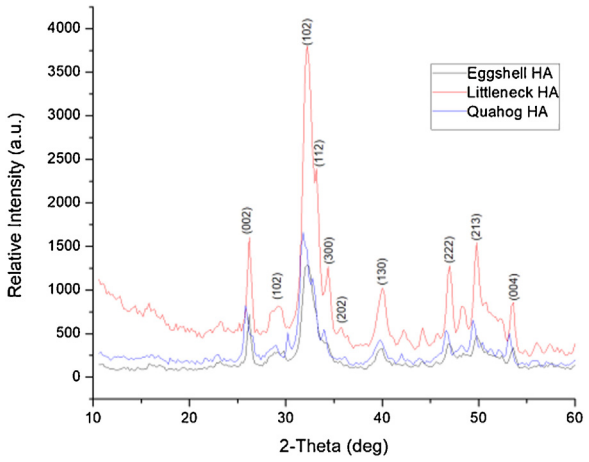

Fig. 2 – X-ray diffraction diffractograms of as-synthesized Eggshell HA, Littleneck HA, and Quahog HA.

and corresponded to polycrystalline hexagonal lattice cells [25]. In each respective XRD pattern, the diffraction peak at 25.88° corresponding to the (002) Miller plane was the most isolated one. The relative intensity of the (002) reflection (66%) was much higher in comparison to the standard XRD pattern of stoichiometric HA (36%). This increase in relative intensity led us to believe that the proposed synthesis favors EnHA crystal growth along the c-axis (JCPDS card no. 00-009-0432) [26]. Out of all 3 samples, the LNnHA XRD pattern had the highest relative intensity while QSnHA had the lowest intensity. The increase in relative intensity indicates that the synthesis technique favors nHA crystal growth along the c-axis [25]. The relative intensities varying from each sample give insight on which EnHA source prefers growth along the c-axis most. This difference in c-axis growth can lead to different particles shapes which will in turn affect the properties of the fabricated scaffolds. These differences in particle shapes can be observed by the HRTEM images. Another unique observation was the broadening of the peak at around 32° in each sample, indicating a small crystalline size of as-synthesized nHA [27]. Because we found that the crystallize size was larger in the [002] crystallographic direction than that of the [300] direction we could imply from this data that the structure of the synthesized EnHA was rod or needle-like. These shapes were later confirmed in SEM images (Fig. 2).

Fig. 3(a–c) shows SEM micrograph images of as-synthesized EnHA. SEM micrographs were used to obtain information on the surface morphology and particle size. Fig. 3(a–c) depicts small particles that occur in clusters. The particles formulating clusters can be attributed to the agglomeration that accompanies nanoparticles with large surface areas. The nHA particles derived from eggshells occurred in elongated lines of rod-like particles while the nHA particles derived from sea shells were also rod shaped but exhibited limited amounts of round, premature particles. Due to the agglomeration the morphologies of the particles were unclear in the SEM micrographs (Fig. 3).

TEM studies were carried out for nanocrystalline HA samples and representative micrographs of ESnHA, LNnHA, and QSnHA are showing in Fig. 4. The HRTEM micrographs revealed

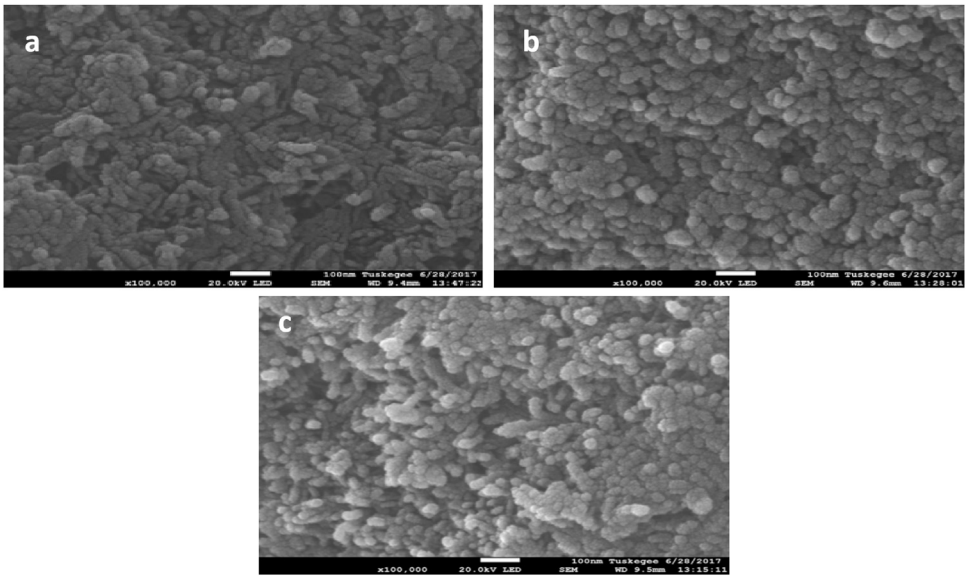

Fig. 3 – Field emission scanning electron microscope micrographs showing as-synthesized Eggshell HA, Littleneck HA, and Quahog HA.

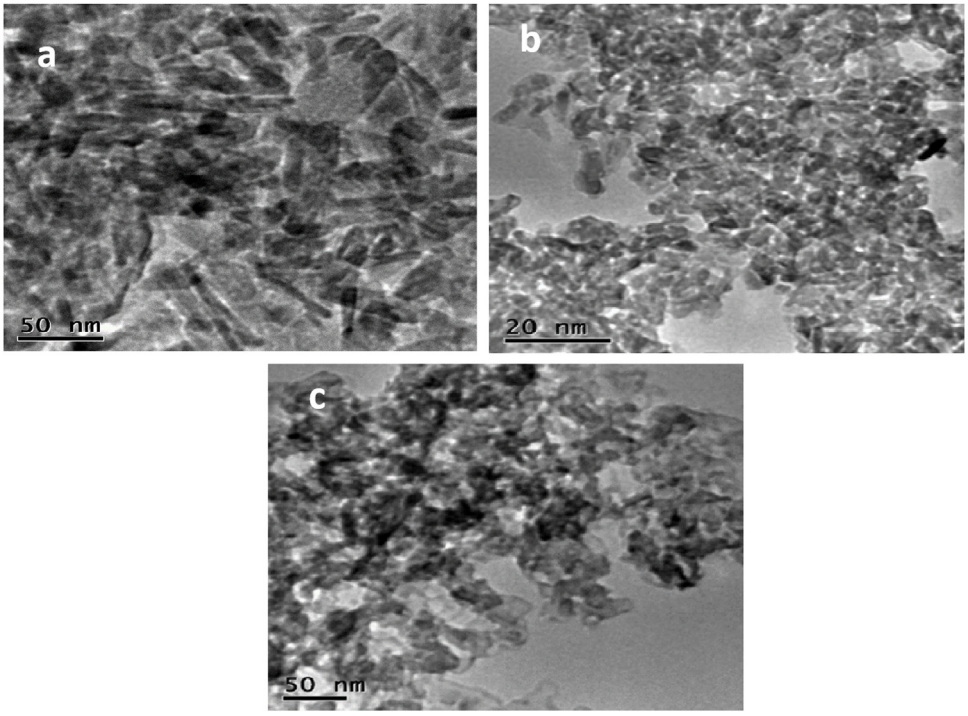

Fig. 4 – High resolution transmission electron microscopy micrographs showing as-synthesized Eggshell HA, Littleneck HA, and Quahog HA.

particles with a needle-like morphology, all with a minimum aggregation. The needle-like shape revealed from the HRTEM images confirmed the XRD analysis which indicated c-axis crystal growth in as-synthesized nHA. LNnHA had the highest relative intensity indicating more c-axis growth will lead to more defined needle-shaped nHA. Based on the HRTEM analysis this can be seen as LNnHA have well defined needle-like nanoparticles that are very small in size. These results are significant as nHA occurs in the form of needle shaped crystals which can lead to enhanced biological properties. As osteoblastic cells can grow and adhere along the c-axis of the particles they can potentially proliferate and differentiate throughout the scaffolds rather than just on top of the surface of the bioactive particles. Based on the results, this synthesis method can be employed to prepare HA particles with controlled shape and morphology. HRTEM micrographs

of as-synthesized QSnHA show particles less needle like but more round and spherical in nature which is to be expected as it exhibited the lowest relative intensity based on XRD results (Fig. 4).

XRD graphs corroborate with this data as the relative intensity was the lowest of each sample indicating a low growth along the c-axis. Round, immature particles can be witnessed in each micrograph but overall the needle shaped particles outnumber the round ones. The evidence from these micrographs shows that the nHA particles are susceptible to a high degree of agglomeration due to the larger surface area of particles. A large surface area provides strong attractive forces between particles and will lead to agglomeration and entanglements. This is something that must be watched closely because if the particles agglomerate during the printing procedure it can disrupt the whole manufacturing process.

3.2. *Physiochemical characterization of the nHA scaffolds*

To investigate the microstructure and surface morphology we utilized SEM; micrographs of each scaffold are displayed in Figs. 4–6. The surface of 3D printed scaffolds shows a rough and irregular surface which can be attributed to the dispersion of nHA and drying as the solution was printed. Stirring was used to prepare nHA based solutions so there may have been an uneven dispersion of the nHA particles within the polymer matrix. Also, as the solutions printed the solvent was still evaporating which led to uneven surfaces on the fibers due to shear-thinning properties. Initially, scaffolds with just 90° alternating layers were produced. After cell-seeding studies it was found that scaffolds with 90° and 45° alternating layers were better for allowing cell adhesion and proliferation as it led to smaller pore sizes and more contact area that seeded cells could adhere and grow on. Tailoring the right percentage of porosity is a parameter that directly affects both mechanical strength and bioactivity. The inter-fiber space within the scaffolds helps to provide an open porous network in a wide variety of options such as pore size and shape. This is directly dependent upon the fiber spacing and printing speed in the individual layer as well as the successive layers. The inter-fibrous porosity is critical to allow tissue in-growth, vascularization, and further tissue remodeling.

3.3. *Biological compatibility of the nHA scaffolds*

To preliminarily examine the potential of our scaffolds for biomedical applications such as tissue-repair and regeneration, interactions between cells and our biomaterials were evaluated on cell-seeded scaffolds by SEM microscopy at different time intervals. Figs. 5–7 show the SEM images of the scaffold surfaces after the indicated periods of incubation. The results of these experiments showed that all 3 scaffolds (Eggshell HA, Fig. 5; Littleneck HA, Fig. 6, and Quahog HA, Fig. 7) could support cell attachment, spreading and growth, without any signs of adverse effects on the cells.

A 70% hydroxyapatite-based slurry composition was prepared by mixing nHA, derived from each respective waste source, and polycaprolactone. HA has proven difficult to print with when using a syringe-based system. To our knowledge this is the first time a scaffold composed of 70% HA has been developed using a wet-syringe based 3D printing method. Using a solution this dense with HA in theory should provide more potential binding sites for cell growth and attachment, Different slurries based on various weight concentrations were prepared to help determine the optimization of printability. Size, shape, and porosity of 3D printed scaffolds can be customized relative to the defect size through the generation of a specific CAD model. The printing nozzle diameter and printing speed was a parameter that directly affected the diameter of a single strand when printing the scaffold structures. This study revealed that conical-shaped micro tips were much more suitable for printing than straight shaped needles. The tapered shape of the conical-shaped micro tips helps facilitate extrusion of the optimum slurry composition [28]. Also, if the printing speed was too high, scaffolds did not have enough time to dry as they were printing which lead to deformed constructs. Another characteristic that was vital to the integrity of the scaffold structure was the average fiber diameter and fiber-to-fiber distance. The optimal average fiber diameter was around 250 μm, also known as the layer thickness. If this property is not tailored just right it will in turn affect properties such as fiber diameter, porosity and just the general overall scaffold integrity. The sources of hydroxyapatite did not have an observable effect on the printability of the scaffolds. Utilizing an extrusion-based system is advantageous as it is a 3D printing process that is easier to adopt than other printing methods and is cost effective [29]. Also, with an extrusion-based printing system the produced scaffolds can be highly customized and fabricated based on the user's scaffold requirements. Parameters such as pore size, shape, and structural integrity can be customized specifically for each patient. This is an advantage that most scaffold fabrication techniques lack.

The surfaces of all 3 scaffolds (ESnHA, QSnHA, and LNnHA) were suitable for cell adhesion and spreading. From day 1, seeded cells displayed outstanding adhesion and long filopodia attachment on the scaffold surface of ESnHA and QSnHA, LNnHA scaffolds. The cell growth was not 100% uniform on all 3 surfaces, but the difference in cellular adhesion among the printed scaffolds can be attributed to the differences in the scaffold surface morphology and cell seeding density. As time progressed, seeded cells began not only attaching to the surface but began forming layers and colonies of cells both on the surface and among the pores of the scaffold. These layers were caused by a ruffling of the cytoplasm and filopodia attachment between neighboring cells after 3 days. On day 5, the cells were flattened out, showing full compatibility with the scaffolds. These hFOB cells show similar growth phenotype when cultured on 2D surfaces such as collagen-treated petridishes. Longer incubations and further examinations will reveal if the cells form a uniformly solid 3D mass. While no spheroid-like structures can be seen, cells on the LNnHA scaffold surface formed apparent 3D microstructures which was formed by layers of cells forming on each other. Such 3D microstructures could potentially serve as additional matrix for cells to grow and populate the scaffolds.

The surface of all 3 scaffolds was smooth before being seeded with fibroblast cells. Once scaffolds were incubated with cells and culture medium, the surfaces of the scaffolds

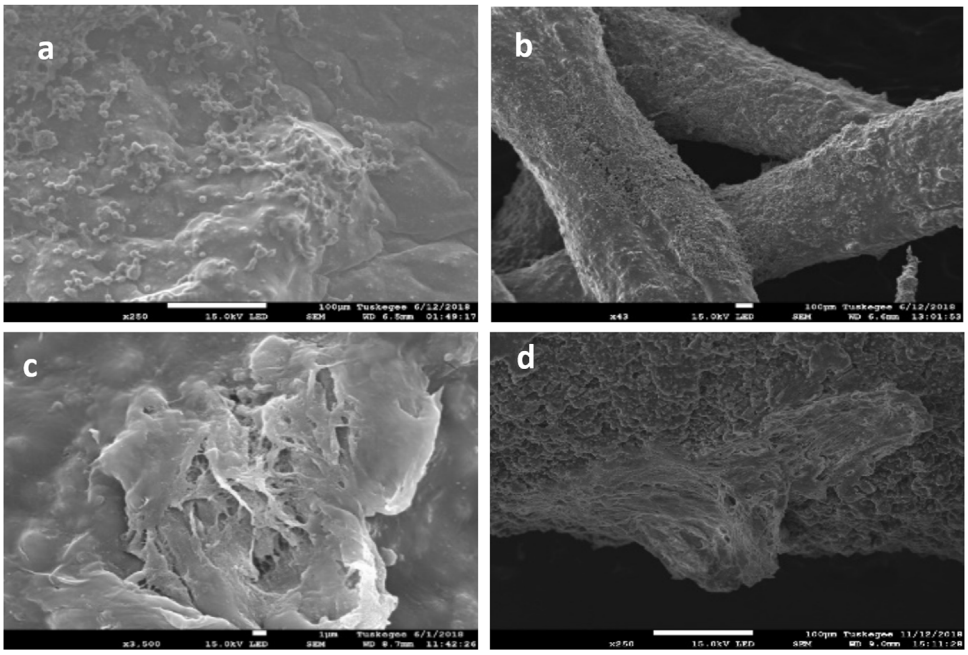

Fig. 5 – FESEM micrographs showing cell interactions on Eggshell HA based scaffold surfaces over various time frames 12 h (a), 1 day (b), 3 days (c), 5 days (d).

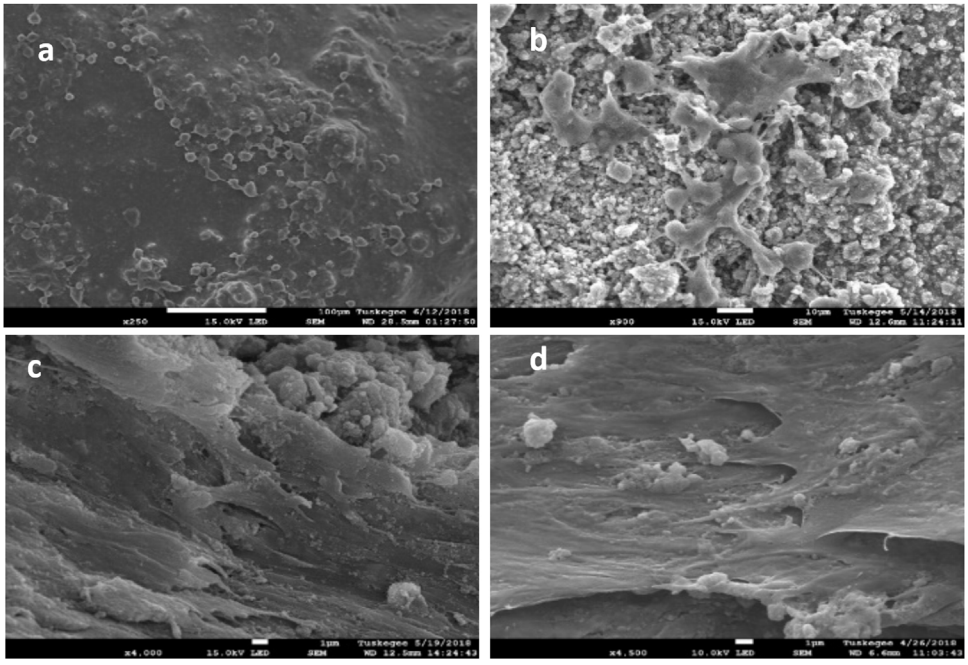

Fig. 6 – FESEM micrographs showing cell interactions on Littleneck HA based scaffold surfaces over various time frames 12 h (a), 1 day (b), 3 days (c), 5 days (d).

began to become coarse, and the micro pores on the surfaces began to disappear. Till day 3, hFOB cells were seen attaching to the surface of the scaffolds. After 3 days' incubation, a thin apatite layer can be seen precipitating on every scaffold surface (Figs. 5–7c), which became more agglomerated on day 5 (Figs. 5–7d). The FESEM images helped show that these scaffolds can adequately serve as an environment where osteoblast cells can grow, attach, and proliferate over various time periods. The scaffolds must be incubated for longer time frames in order to determine how well they can last within the human body.

Previous studies have shown that biocompatibility and bioactivity can be affected by the presence of minor elements that are present within the marine environment [30]. When

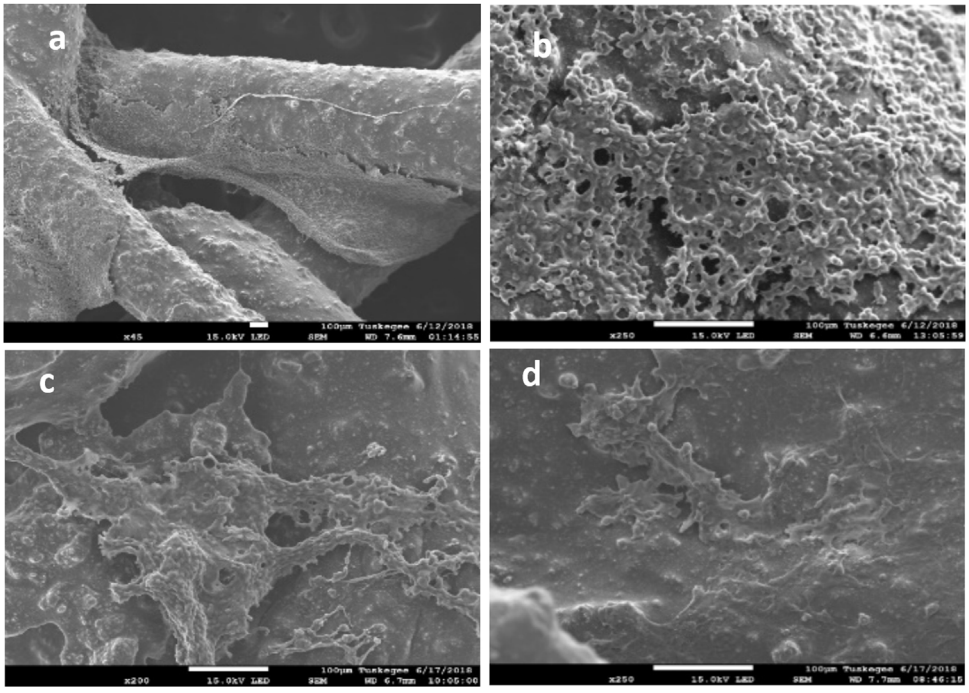

Fig. 7 – FESEM micrographs showing cell interactions on Quahog HA based scaffold surfaces over various time frames 12 h (a), 1 day (b), 3 days (c), 5 days (d).

seashells are converted into biocompatible HA they possess better biological properties as they harbor beneficial cations like Mg^{2+}, Al^{3+}, Sr^{2+}, Zn^{2+}, K^{+}, and Na along with beneficial anions like Cl-, and F-. When both of these cations and anions are used in conjunction it is reported that they aid to facilitate rapid bone regeneration. Due to these studies, this led to the conclusion that nHA derived from sea-shell waste was better at producing greater amounts of cell attachment and growth. Future studies will employ longer and more in-depth cell studies to determine if this is the case.

3.4. *Mechanical assessment of the EnHA based scaffolds*

The structural integrity of the PCL/EnHA based scaffolds as potential bone replacements was evaluated and characterized using tensile strength tests. Fig. 8 displays the representative stress versus strain responses of the 3D printed 70 wt% PCL and 30 wt% EnHA scaffolds produced from the three respective waste sources. The two scaffolds that featured EnHA derived from seashells demonstrated similar fracture behaviors. An initial elastic response is observed, followed by plastic deformation and then finally the samples failed [31]. This is a typical response when it comes to materials highly porous in nature. The EnHA derived from eggshell had a very different response, it behaved in a very brittle manner. It exhibited no plastic deformation whatsoever; the sample quickly reached the ultimate tensile strength before failing.(Table 2)

Additionally, ultimate tensile strength varied although the tested samples all contained the same amount of EnHA particles (70 wt%). The ultimate tensile strength for the LNnHA based scaffolds was the highest at 20.76 ± 4.56 MPa, next was

Table 2 – Ultimate tensile strength of the PCL/EnNA scaffold produced from various waste sources; eggshell (ESnHA), littleneck clam shells (LNnHA), and quahog clam shells (QSnHA).

Sample	Tensile modulus (MPa)	Ultimate tensile strength (MPa)	% Strain
ESnHA	67.36 ± 10.43	5.83 ± 1.36	11.20 ± 2.47
QSnHA	208.00 ± 07.64	12.60 ± 0.12	14.00 ± 1.41
LNnHA	434.80 ± 52.44	20.76 ± 4.56	12.80 ± 2.19

QSnHA with an ultimate tensile strength of 12.60 ± 0.12 MPa, the worst performing scaffold, ESnHa had an ultimate tensile strength of 5.83 ± 1.36 MPa. There are a few factors that can be attributed to the varying ultimate tensile strength. The first factor is the uniform distribution of still HA particles in the PCL polymer. It is well accepted that by incorporating fillers as reinforcements an effective means of enhancing themechanical strength of polymers can be obtained [32]. A more uniform distribution of the EnHA particles in the polymer is the likely reason for an enhancement in mechanical properties [33]. HA phase is known that possess a much higher stiffness that a flexible polymer such as PCL, this increase in stiffness allows it to retain applied loads, which is often seen in the case of organic/inorganic composites [34,35]. Although each scaffold contained EnHA, each EnHA was derived from a different source and all had distinct physiochemical properties. Although the manufactured scaffolds possessed adequate biological and mechanical properties for applications such as bone and dental tissue regeneration, there are still various scopes of the work that can be investigated. One property that was not study in this project was that of interfacial adhe-

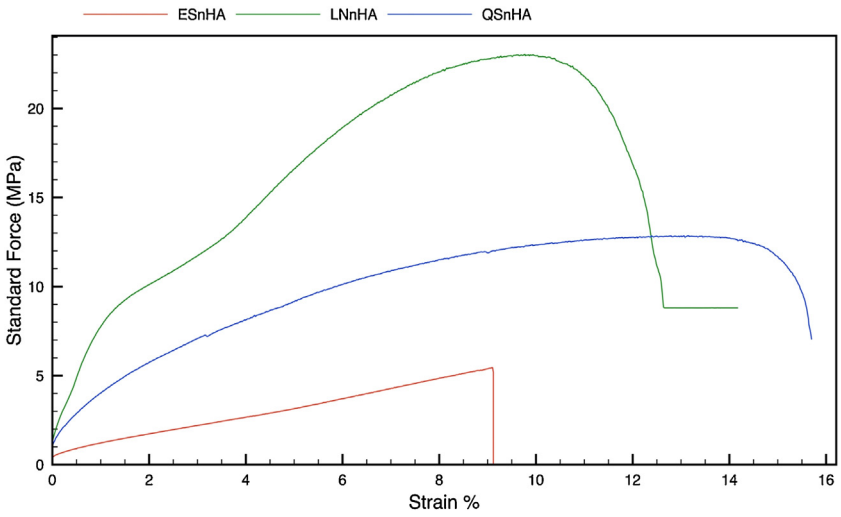

Fig. 8 – Representative stress versus strain responses of the PCL/EnNA scaffold produced from various waste sources; eggshell (ESnHA), littleneck clam shells (LNnHA), and quahog clam shells (QSnHA).

sion. Due to the hydrophobicity of PCL and hydrophilicity of HA when the two are used in conjunction, problems are known to arise such as weak interfacial bonding and agglomeration [36,37]. Lack of adhesion between the polymer phase and bioactive fillers can result in early failure at the interface, which leads to poor mechanical properties [38]. Future work is being done to tailor the surface properties of biomaterials using low temperature plasma to increase interfacial adhesion. Using plasma as a surface treatment technique can potentially change the PCL surface from hydrophobic to hydrophilic which can in turn lead to increased interfacial adhesion and enhanced mechanical properties.

Companies are desperately seeking ways to optimize manufacturing processes to reduce energy consumption and waste. As we strive for an environmentally sustainable future, utilizing waste to produce valuable biomaterials is a promising trend. 3D printing is emerging as a sustainable technology, primarily due to two benefits: it facilitates more efficient designs and creates less waste [39]. By utilizing egg and seashell waste as a key material component within an already sustainable manufacturing technique, it further alleviates the stresses put on the economy and environment.

4. Conclusion

Composite scaffolds were successfully produced by 3D printing hydroxyapatite-based slurries derived from eggshell and seashell waste sources. Scaffolds with various pore types and inter-dimensional shapes were produced which can lead to patient specific shaped scaffolds. Hydroxyapatite was derived from three sources of naturally occurring shell waste. nHA derived from each waste source provided highly bioactive and biocompatible properties that allowed osteoblast cells the ability to adhere and proliferate over various time frames. The incorporation of polycaprolactone served as a suitable polymer matrix and helped improve the printability and flowability of the nHA slurries. Waste materials are an abundant sustainable source for value-added 3D printing materials with bioactive properties.

Author contributions

The manuscript was written through contributions of all authors. All authors have given approval to the final version of the manuscript.

Conflicts of interest

The authors declare no conflicts of interest.

Acknowledgements

The authors acknowledge the financial support of NSF-AL-EPSCoR# 1655280, NSF-RISE #1459007, NSF-CREST#, 1735971 and NSF-MRI-1531934.

REFERENCES

[1] Quina MJ, Soares MAR, Quinta-Ferreira R. Applications of industrial eggshell as a valuable anthropogenic resource. Resour Conserv Recycl 2017;123:176–86.
[2] Meng X, Deng D. Trash to treasure: waste eggshells used as reactor and template for synthesis of Co9S8 nanorod arrays on carbon fibers for energy storage. Chem Mater 2016;28:3897–904.
[3] Radziemska M, Vaverková MD, Adamcová D, Brtnický M, Mazur Z. Valorization of fish waste compost as a fertilizer for agricultural use. Waste Biomass Valorization 2019;10:2537–45.
[4] Adeogun AI, Ofudje AE, Idowu MA, Kareem SO. Facile development of nano size calcium hydroxyapatite based ceramic from eggshells: synthesis and characterization. Waste Biomass Valorization 2018;9:1469–73.

[5] De Angelis G, Medeghini L, Conte AM, Mignardi S. Recycling of eggshell waste into low-cost adsorbent for Ni removal from wastewater. J Clean Prod 2017;164. Elsevier Ltd.
[6] Mo KH, Alengaram UJ, Jumaat MZ, Lee SC, Goh WI, Yuen CW. Recycling of seashell waste in concrete: a review. Constr Build Mater 2018;162:751–64.
[7] Yao Z, et al. Bivalve shell: not an abundant useless waste but a functional and versatile biomaterial. Crit Rev Environ Sci Technol 2014;44:2502–30.
[8] Idaszek J, Kijeńska E, Łojkowski M, Święszkowski W. How important are scaffolds and their surface properties in regenerative medicine. Appl Surf Sci 2016;388:762–74, http://dx.doi.org/10.1016/j.apsusc.2016.03.038.
[9] Kijeńska E, Zhang S, Prabhakaran MP, Ramakrishna S, Swieszkowski W. Nanoengineered biocomposite tricomponent polymer based matrices for bone tissue engineering. Int J Polym Mater Polym Biomater 2016;65:807–15.
[10] Oberbek P, et al. Characterization and influence of hydroxyapatite nanopowders on living cells. Beilstein J Nanotechnol 2018;9:3079–94.
[11] Dulinska-Molak I, Mao H, Kawazoe N, Chen G. Effect of single-wall carbon nanotubes on mechanical property of chondrocytes. J Nanosci Nanotechnol 2014;14:2459–65.
[12] Cheng Liang-Chien, Jiang Xiumei, Jing Wang CC, R-SL. Nanoscale. Nanoscale 2013;(9):3–10.
[13] Nomura K, Terwilliger P. Self-dual leonard pairs biocomposite scaffold preparation from hydroxyapatite extracted from waste bovine; 2020. p. 37–47.
[14] Huang R, Zhu X, Tu H, Wan A. The crystallization behavior of porous PLA prepared by modified solvent casting/particulate leaching technique for potential use of tissue engineering scaffold. Mater Lett 2014;136:126–9, http://dx.doi.org/10.1016/j.matlet.2014.08.044.
[15] Patrício T, Domingos M, Gloria A, Bártolo P. Characterisation of PCL and PCL/PLA scaffolds for tissue engineering. Procedia CIRP 2013;5:110–4.
[16] Johari N, Fathi MH, Golozar MA. Fabrication, characterization and evaluation of the mechanical properties of poly (-caprolactone)/nano-fluoridated hydroxyapatite scaffold for bone tissue engineering. Compos B Eng 2012;43:1671–5.
[17] Zhu X, Zhong T, Huang R, Wan A. Preparation of hydrophilic poly(lactic acid) tissue engineering scaffold via (PLA)-(PLA-b-PEG)-(PEG) solution casting and thermal-induced surface structural transformation. J Biomater Sci Polym Ed 2015;26:1286–96.
[18] Tabassum S, et al. Efficient drug delivery system for bone repair by tuning the surface of hydroxyapatite particles. RSC Adv 2016;6:104969–78.
[19] Pramanik N, Imae T. Fabrication and characterization of dendrimer-functionalized mesoporous hydroxyapatite. Langmuir 2012;28:14018–27.
[20] Khajavi R, Abbasipour M, Bahador A. Electrospun biodegradable nanofibers scaffolds for bone tissue engineering. J Appl Polym Sci 2016;133.
[21] Loh QL, Choong C. Three-dimensional scaffolds for tissue engineering applications: role of porosity and pore size. Tissue Eng B Rev 2013;19:485–502.
[22] Shuai Cijun, Liu Guofeng, Yang Youwen, Qi Fangwei, Peng Shuping, Yang Wenjing, et al. A strawberry-like Ag-decorated barium titanate enhances piezoelectric and antibacterial activities of polymer scaffold. Nano Energy 2020;74:104825.
[23] Yang Youwen, Lu Changfu, Peng Shuping, Shen Lida, Wang Di, Qi Fangwei, et al. Laser additive manufacturing of Mg-based composite with improved degradation behaviour. Virtual Phys Prototyp 2020;15(3):278–93.
[24] Yang S, Leong K-F, Du Z, Chua C-K. The design of scaffolds for use in tissue engineering. Part II. Rapid prototyping techniques. Tissue Eng 2002;8:1–11.
[25] Puvvada N, Panigrahi PK, Pathak A. Room temperature synthesis of highly hemocompatible hydroxyapatite, study of their physical properties and spectroscopic correlation of particle size. Nanoscale 2010;2:2631–8.
[26] Xue M, et al. Structure, hydrogen storage, and luminescence properties of three 3D metal-organic frameworks with NbO and PtS topologies. Cryst Growth Des 2008;8: 2478–83.
[27] Zhang Y, Lu J. A mild and efficient biomimetic synthesis of rodlike hydroxyapatite particles with a high aspect ratio using polyvinylpyrrolidone as capping agent. Cryst Growth Des 2008;8:2101–7.
[28] Dadhich P, et al. A simple approach for an eggshell-based 3D-Printed osteoinductive multiphasic calcium phosphate scaffold. ACS Appl Mater Interfaces 2016;8: 11910–24.
[29] Vaezi M, Zhong G, Kalami H, Yang S. Extrusion-based 3D printing technologies for 3D scaffold engineering. In: Functional 3D tissue engineering scaffolds: materials, technologies, and applications. Elsevier Ltd; 2018, http://dx.doi.org/10.1016/B978-0-08-100979-6.00010-0.
[30] Hadagalli K, Panda AK, Mandal S, Basu B. Faster biomineralization and tailored mechanical properties of marine-resource-derived hydroxyapatite scaffolds with tunable interconnected porous architecture. ACS Appl Biol Mater 2019;2:2171–84.
[31] Gloria A, De Santis R, Ambrosio L. Polymer-based composite scaffolds for tissue engineering. J Appl Biomater Biomech 2010;8:57–67.
[32] Yang Y, et al. Metal organic frameworks as a compatible reinforcement in a biopolymer bone scaffold. Mater Chem Front 2020;4:973–84.
[33] Mo KH, et al. Recycling of seashell waste in concrete: a review. Constr Build Mater 2018;162:751–64.
[34] Wagoner Johnson AJ, Herschler BA. A review of the mechanical behavior of CaP and CaP/polymer composites for applications in bone replacement and repair. Acta Biomater 2011;7:16–30.
[35] Li JJ, Kaplan DL, Zreiqat H. Scaffold-based regeneration of skeletal tissues to meet clinical challenges. J Mater Chem B 2014;2:7272–306.
[36] Wang MO, et al. Evaluating 3D-printed biomaterials as scaffolds for vascularized bone tissue engineering. Adv Mater 2014;27:138–44.
[37] Abboud M, Turner M, Duguet E, Fontanille M. PMMA-based composite materials with reactive ceramic fillers Part 1. - chemical modification and characterisation of ceramic particles. J Mater Chem 1997;7:1527–32.
[38] Liang JZ. Toughening and reinforcing in rigid inorganic particulate filled poly(propylene): a review. J Appl Polym Sci 2002;83:1547–55.
[39] Allen D, et al. Sustainable materials management: the road ahead. Packag Bost Mass 2009:1–49.